L1 Unmixing and its Application to Hyperspectral Image Enhancement

Zhaohui Guo, Todd Wittman and Stanley Osher

Univ. of California, 520 Portola Plaza , Los Angeles, CA 90095, USA

ABSTRACT

Because hyperspectral imagery is generally low resolution, it is possible for one pixel in the image to contain several materials. The process of determining the abundance of representative materials in a single pixel is called spectral unmixing. We discuss the L1 unmixing model and fast computational approaches based on Bregman iteration. We then use the unmixing information and Total Variation (TV) minimization to produce a higher resolution hyperspectral image in which each pixel is driven towards a "pure" material. This method produces images with higher visual quality and can be used to indicate the subpixel location of features.

Keywords: Hyperspectral imagery, spectral unmixing, image super-resolution, total variation

1. INTRODUCTION

The main advantage of using hyperspectral imagery is that the spectral signature of each pixel can help identify the materials in the scene. However, precise spectral information generally comes at the cost of low spatial image resolution. There have been several methods proposed to enhance the spatial resolution of hyperspectral images. Most of these methods are based on fusing the hyperspectral image with a higher resolution in a different modality. Hyperspectral images have been effectively sharpened using high resolution multispectral images,[1,2] panchromatic images,[3] and aerial photographs.[4] Of course, these methods assume that corresponding scene data is available and that the images can be precisely co-registered.

The goal of this paper is to enhance the spatial resolution of hyperspectral images using the detailed spectral information of the image. As a first step, each pixel in the hyperspectral image should be separated into its component materials, a process known as spectral unmixing. Once the materials present in each pixel are identified, our goal is to zoom the image to the point where each pixel is "pure," meaning each pixel in the image consists of a single material. To accomplish this we present an energy-based image zooming model that incorporates the spectral signatures of target materials. The resulting image has enhanced spatial quality and can reveal features that were not present in the original hyperspectral image, provided that the features were adequately described by the unmixing process.

In the next section, we briefly review spectral unmixing and describe the L1 unmixing model used in this paper. In Section 3, we introduce two energy-based models for resolution enhancement, one model encouraging pixel purity and the other model strictly enforcing it. We present results on HYDICE images in Section 4 and conclude by suggesting directions for further research.

2. SPECTRAL UNMIXING

Because hyperspectral images are typically low resolution, around 3-4m resolution for HYDICE images, it is reasonable to assume that a single pixel may contain several different materials, each possessing a different hyperspectral signature. Spectral unmixing breaks down a single pixel's spectral signal into a combination of materials. The representative material signatures are called endmembers and are generally known a priori. The endmembers may be drawn from a spectral library or codebook, but more commonly the endmembers

Send correspondence to Todd Wittman.
Zhaohui Guo: annegzh@math.ucla.edu
Todd Wittman: wittman@math.ucla.edu
Stanley Osher: sjo@math.ucla.edu

are selected from the image itself to ensure spectral coherence. There are several algorithms for endmember selection, including N-FINDR,[5] Pixel Purity Index,[6] simplex methods,[7] iterative basis pursuit,[8] and careful manual selection.[9] The endmember signals should possess distinct shapes so that we can separate out different materials. Ideally, the endmember set will be small but the signals still well describe all mixed pixels in the image.

Let $\{m_i\}_{1\leq i\leq N}$ denote the set of N endmember material signals. We will arrange the signals m_i as the columns of the endmember matrix M. The goal of an unmixing model is to identify the abundance a_i of each endmember m_i such that the combination forms a given signal f. We will write the abundance values $a_1, ..., a_N$ as a column vector a. For mathematical simplicity, it is common to assume a linear mixing model:

$$f \approx \sum_{i=1}^{N} m_i a_i = Ma.$$

We will adopt the linear mixing model in this paper, but we should note that analysis of the physics involved in image formation indicates the mixing is actually nonlinear.[10] For more information on spectral mixing, consult the survey article by Keshava and Mustard.[11]

2.1 Least Squares Unmixing

The most straightforward approach to solving the linear problem $f \approx Ma$ is by Least Squares (LS) minimization:

$$\min_a \|Ma - f\|_2^2 .$$

The abundance vector a can be obtained directly by the formula

$$a = (M^T M)^{-1} M^T f.$$

However, this solution may produce negative abundance values, which is physically unrealistic. Furthermore, the LS solution is well-known to be dense, in the sense that the almost every abundance a_i will be non-zero. The basic problem arises from the fact that the endmember set $\{m_i\}_{i=1}^N$ does not form a complete basis that spans the image space. In practice, we will almost surely never achieve equality $f = Ma$.

A common correction for these issues is to impose constraints to obtain the Constrained Least Squares (CLS) model:

$$\min_a \|Ma - f\|_2^2 \quad \text{subject to} \quad a_i \geq 0,\ \sum_{i=1}^{N} a_i = 1. \tag{1}$$

Minimization approaches for CLS include gradient descent[12] and Orthogonal Subspace Projection.[13] The CLS model enforces non-negativity and tends to produce sparse solutions, in the sense that it produces only a few coefficient $a_i \geq 0$. The reasoning behind the sum-to-one constraint is that the abundances a_i represent fractional values or percentages that must add up to 100%. However, this constraint is unphysical as the coefficients a_i just indicate the amount of a material's contribution in a linear combination; there is no reason to assume a_i represents a percentage. In practice, the sum of the abundance values will be close to 1 because the endmembers are generally drawn from the image itself and the signals have roughly the same magnitude. The values will almost never sum to exactly 1 and may sum to a very different value if the endmembers m_i were drawn from a different source such as a spectral library. To meet the sum-to-one constraint, a common adjustment is to add a near-zero "shade" endmember to the matrix M.

2.2 The Least Squares L1 (LSL1) Model

The goal is to produce a solution a that is sparse while still respecting $f \approx Ma$. Inspired by recent work in compressive sensing, we minimize the L1-norm of the abundance vector a. We propose the Least Squares L1 (LSL1) model:

$$\min_a \|a\|_1 + \frac{\lambda}{2} \|Ma - f\|_2^2 \quad \text{subject to } a_i \geq 0. \tag{2}$$

In the above equation, λ is a parameter that balances the sparsity of the solution and the how closely the endmembers describe the signal f. The choice of λ will depend on how well the endmembers represent the image data. This model does not enforce the sum-to-one constraint, which means computational adjustments such as the shade endmember should be unnecessary. There is a connection between the L1-norm and the sum-to-one constraint which explains why the CLS model tends to give sparse solutions. If we assume all coefficients $a_i \geq 0$, then the L1-norm $\|a\|_1 = \sum a_i$. So the CLS model keeps the L1-norm small by enforcing $||a||_1 = 1$. The LSL1 model (2) can be seen as a relaxation of the CLS model (1). Instead of strictly enforcing $\|a\|_1 = 1$, the LSL1 model makes $\|a\|_1$ minimal.

There are several efficient calculus-based methods for the minimization in (2). The simplest minimization scheme is by gradient descent. Introducing an artificial time dependent parameter t, we evolve the differential equation

$$\frac{\partial a}{\partial t} = -\text{sgn}(a) - \lambda M^T(Ma - f). \tag{3}$$

The discontinuity in the *sgn* function can be problematic numerically. It can be approximated by the arctangent function

$$\text{sgn}(a) \approx \frac{2}{\pi} \arctan\left(\frac{a}{\epsilon}\right)$$

where $\epsilon > 0$ is a small value. Discretizing equation (3) with a time step Δt yields an iterative update scheme:

$$a^{n+1} = a^n - \Delta t \left(\frac{2}{\pi} \arctan\left(\frac{a}{\epsilon}\right) + \lambda M^T(Ma - f) \right).$$

To enforce the non-negativity constraint $a_i \geq 0$, we threshold the components of a at each iteration

$$a_i^{n+1} = \max\left(a_i^{n+1}, 0\right).$$

The scheme can be initialized $a^0 = 0$. The iterations can be stopped after a fixed number of iterations or when the norm of the update $\left\|a^{n+1} - a^n\right\|_2$ is below some threshold. While this scheme is easy to program, it is not stable for small values of λ.

There are a suite of methods designed for the compressed sensing problem based on Bregman iteration which can be applied to the unmixing problem.[14,15] These methods should outperform gradient descent in terms of speed for problems closely related to the minimization in (2). One such iterative scheme is the Split Bregman method developed recently by Goldstein and Osher.[16] For a given signal f, the Split Bregman algorithm initializes the variables

$$a^0 = b^0 = d^0 = 0, \ f^0 = f.$$

Then for a choice of parameters μ and γ, we update the variables by

$$\begin{aligned} b^{n+1} &= b^n + a^n - d^n \\ a^{n+1} &= \left(M^T M + \gamma I\right)^{-1} \left(M^T f^n - b^{n+1} + d^n\right) \\ d^{n+1} &= \max\left(a^{n+1} + b^{n+1} - \mu, 0\right). \end{aligned}$$

The Bregman iterative methods will achieve faster convergence if we "add the noise back" after achieving a local minimum. At fixed intervals in the iterative process (not at every iteration), we update f^n by

$$f^{n+1} = f^n + f - Ma^{n+1}.$$

The parameter μ is a thresholding parameter that is usually chosen to be small. The parameter γ balances the sparsity of the result, similar to the effect of λ in equation (2). We have found that the value

$$\gamma = \frac{10}{|M^T M\|_2}$$

works well for real data.

For a derivation of these equations and convergence analysis, we refer the reader to the paper by Goldstein and Osher.[16] The Split Bregman minimization is numerically stable for all values of γ. On real data, Split Bregman converges for a single image pixel about 20 times faster than gradient descent. When applied to an image with a large number of pixels, this improvement in runtime becomes considerable. The Split Bregman method also tends to give better results than gradient descent in terms of sparsity and noise removal.

3. HYPERSPECTRAL IMAGE ENHANCEMENT

After spectral unmixing has been applied to each pixel in the image, we can enhance the hyperspectral image using the information about the materials present in the scene. Let $f : \Re^d \to \Lambda$ be the original d-dimensional hyperspectral image defined on some low resolution domain Λ. We wish to produce a high resolution image $u : \Re^d \to \Omega$ on a higher resolution domain Ω. Generally, Λ is a rectangular grid and Ω is obtained by expanding the grid by some integer magnification factor.

3.1 The Total Variation (TV) Energy

Assume that the optical blur process can be described by a linear convolution with a known point-spread function (PSF). We will further assume the PSF is a Gaussian kernel G_σ with known standard deviation σ. To match the images u and f over all image bands $1 \leq j \leq d$, we minimize the quantity

$$\sum_{j=1}^{d} \int_\Omega \left(G_\sigma * u_j - \uparrow f_j\right)^2 dx \tag{4}$$

where $\uparrow$ denotes the upsampling operation. Note this term is the sum over all the bands of the least squares fit between each image band. This quantity is often referred to as the fidelity or matching term.

The term (4) describes possible pixel values $u(x)$, but the choice of values and the particular arrangement on the high resolution grid is non-unique. Therefore, it is common to add a regularization term to the minimization of (4). A natural choice for arranging the pixels is to assume that similar materials will be more likely to be adjacent than spectrally disparate materials. A common approach for measuring the difference between neighboring pixels is to examine the image gradient $\nabla u = \left\langle \frac{\partial u}{\partial x}, \frac{\partial u}{\partial y} \right\rangle$. The smoothness of the image u can be quantified by the L2-norm of the gradient, summed over all pixels x and all bands j:

$$\sum_{j=1}^{d} \int_\Omega \|\nabla u_j\|_2 \, dx. \tag{5}$$

For grayscale images with $d = 1$, this term is known as the Rudin-Osher-Fatemi Total Variation (TV) norm.[17] In general, a small value for (5) would indicate a smooth or piecewise constant image, while a large value would indicate a highly textured or noisy image.

Putting together terms (4) and (5), we obtain the classical TV energy. The zooming model can be then written as the minimization of the energy

$$\min_u E[u] = \sum_{j=1}^{d} \int_\Omega \|\nabla u_j\|_2 \, dx + \frac{\alpha}{2} \sum_{j=1}^{d} \int_\Omega \left(G_\sigma * u_j - \uparrow f_j\right)^2 dx. \tag{6}$$

where α is a parameter balancing the two terms. The value of α is usually set experimentally, although there are automated methods for setting the parameter.[18] This energy has been well-studied and has been shown to be effective for image deblurring and upsampling.[19–21] Minimizing (6) should interpolate the image, but it does not make use of the spectral information derived from the unmixing process.

If the endmembers m_i describe the image scene completely and the magnification factor is chosen large enough, we can reasonably expect each pixel in the high resolution image to be pure: $u(x) \in \{m_i\}_{i=1}^N$. Let $I(x)$ denote the indices of the endmembers detected by the unmixing process to have positive abundance at pixel x:

$$I(x) = \{i : 1 \leq i \leq N, a_i(x) > 0\}.$$

In other words, $I(x)$ indicates which materials were present in the scene at a particular location. We wish to incorporate this information into the TV zooming energy (6) so that the resulting pixel values $u(x)$ closely resemble the detected endmember signals. This can be done in two ways: a "soft" version that encourages endmember signals and a "hard" version that strictly requires each pixel to be an endmember signal.

3.2 The Endmember-Based TV Model

The "soft" version can be implemented by adding a term to (6) that penalizes deviation from the detected endmember signals $\{m_i, i \in I(x)\}$. We propose the *Endmember-Based TV* model as

$$\min_u E[u] = \sum_{j=1}^{d} \int_\Omega \|\nabla u_j\|_2 \, dx + \frac{\alpha}{2} \sum_{j=1}^{d} \int_\Omega \left(G_\sigma * u_j - \uparrow f_j\right)^2 dx + \frac{\beta}{2} \int_\Omega \prod_{i \in I(x)} \|u - m_i\|_2^2 . \tag{7}$$

The parameter β controls how strictly the endmember signals should be matched. Calculating the Euler-Lagrange equation, the first variation of energy is

$$\nabla E = -\sum_{j=1}^{d} \int_\Omega \nabla \cdot \left(\frac{\nabla u_j}{\|\nabla u_j\|_2} \right) + \alpha \sum_{j=1}^{d} \int_\Omega G_\sigma^* * \left(G_\sigma * u_j - \uparrow f_j\right) dx + \beta \int_\Omega \sum_{k \in I(x)} \prod_{i \in I(x)} \frac{\|u - m_i\|_2^2}{\|u - m_k\|_2}. \tag{8}$$

The energy (7) can then be minimized by evolving the gradient descent equation

$$\frac{\partial u}{\partial t} = -\nabla E.$$

For an appropriately chosen time step Δt, this scheme will converge to a high resolution image u with each pixel resembling an endmember detected by the unmixing procedure. However, the third term enforcing endmember matching is non-convex. This means the gradient descent scheme will only converge to a solution for small vales of the parameter β. The energy (7) can be minimized by more sophisticated numerical methods, such as Split Bregman iteration,[16] that will permit a wider range of values for β.

3.3 The Quantum TV Model

The "hard" version of the TV model will strictly require each value $u(x)$ in the final image to be one of the detected endmember signals. For grayscale images, TV minimization over a set of fixed gray values is called *Quantum TV* minimization and was studied by Shen and Kang.[22] Extending Shen and Kang's model to hyperspectral images, we obtain the following iterative update scheme:

$$v^{n+1} = \arg\min_u \sum_{j=1}^{d} \int_\Omega \|\nabla u_j\|_2 \, dx + \frac{\alpha}{2} \sum_{j=1}^{d} \int_\Omega \left(G_\sigma * u_j - \uparrow f_j\right)^2 dx \tag{9}$$

$$u^{n+1}(x) = \arg \min_{\{m_i(x):\, i \in I(x)\}} \left\| m_i(x) - v^{n+1}(x) \right\|_2 . \tag{10}$$

This scheme is an alternating minimization that first finds the image that minimizes the standard TV energy in (6) and then rounds each pixel $u(x)$ to the nearest endmember signal in $I(x)$. In practice, the model will converge in two or three iterations on real data. The TV minimization in the first step (9) can be performed by a gradient descent scheme using the first two terms of (8) or by a Split Bregman method similar to the scheme described in Section 2.[16]

The images that result from the Quantum TV model will look radically different from the original data f. This is because the pixels in the original data were mixed, while each pixel in the final image u must be pure. The result of the Quantum TV model should be interpreted as a segmentation or classification map, while the result of the Endmember-Based TV model is an image enhancement. The classification produced by the Quantum TV model is at a higher resolution than the original image, so the result may provide more precise spatial information than a classification map derived from the original data.

4. NUMERICAL RESULTS

In this section we present some numerical results for hyperspectral unmixing and image enhancement. The data under consideration is a HYDICE hyperspectral image called Urban which is publicly avaiable.[23] After removing the water absorption bands, Urban is a 163-band image. We chose 6 endmembers from the image using N-FINDR[5] plus manual adjustment. The endmembers selected and their spectral signatures are shown in Figure 1.

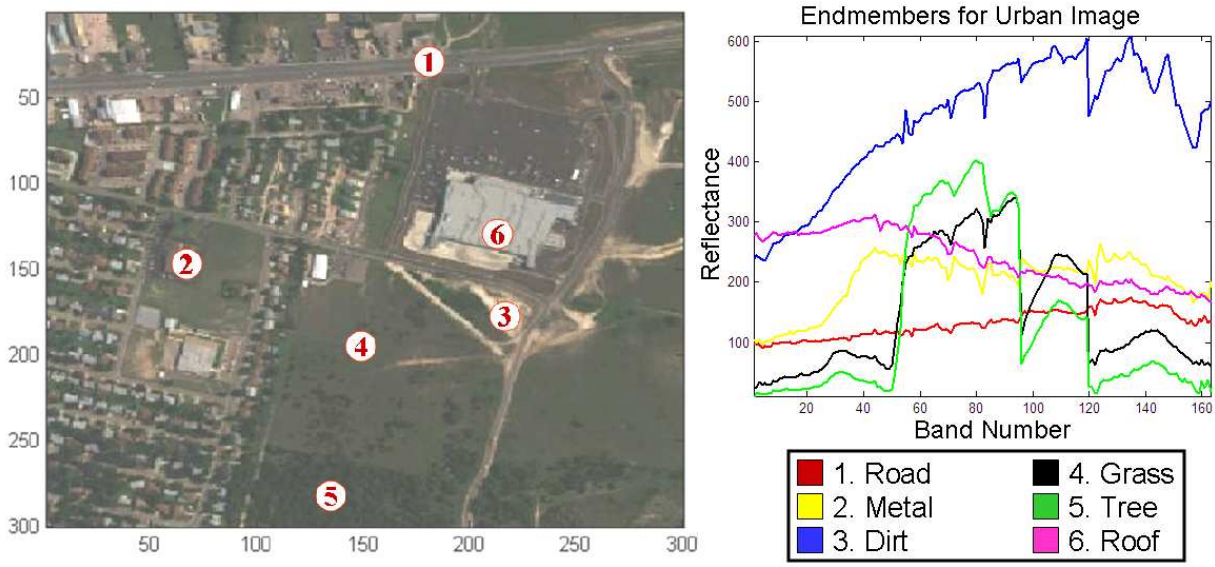

Figure 1. Endmember selection on the Urban image. Left: The pixels selected as endmembers. Right: The spectral signatures of the endmembers.

4.1 Spectral Unmixing Results

We performed linear spectral unmixing using the LSL1 model described in Section 2.2. The minimization was carried out by the Split Bregman method with a fixed number of iterations. We chose the parameters $\gamma = 5\times10^{-7}$ and $\mu = 0.1$. The computation takes approximately 0.01 seconds to unmix each pixel in the image, running on a dual core desktop with 2.99GHz processor and 1.96GB memory.

The six fraction planes indicating the abundance of each endmember are shown in Figure 2. Qualitatively, the unmixing result appears to be correct. The fraction planes effectively segment the roads and buildings in the original image. Pixels that appear bright in more than one fraction plane indicate a mixture of several materials. For example, the region in the lower right quadrant appears to be a mixture of dirt, grass, and trees.

4.2 Image Enhancement Results

Using the unmixing results obtained in Section 4.1, we can enhance the hyperspectral image using the Endmember-Based and Quantum TV models. To illustrate the difference between these models, we first prepared the 177-band synthetic 2x2 hyperspectral image shown in Figure 3. Each pixel in the image is a linear combination of 4 distinct spectral signatures taken from a spectral library. The pixels in the lower left and upper right corners are mostly the light blue material mixed with a smaller portion of the green material. The pixel in the upper left corner is an equal mixture of the dark blue and green materials. Finally, the pixel in the lower right is primarily the light blue material mixed with a small portion representing the purple material. This fourth pixel represents a subpixel anomaly in the image. The 2x2 image was zoomed by a factor of 4 using both models to obtain 8x8 images. The Endmember-Based TV result is a smooth image with blurry material boundaries. In a larger image, this may correspond to a visually pleasing result. The Quantum TV result is a classification map, with each

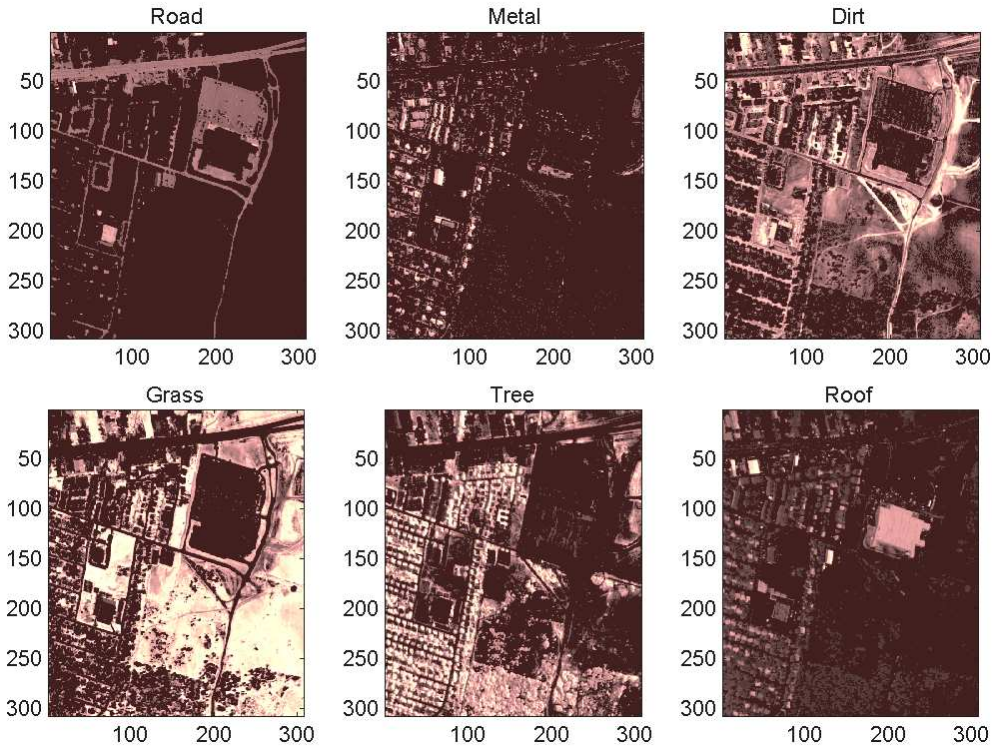

Figure 2. Fraction planes of the Urban image indicating the abundances detected by LSL1 unmixing using the Split Bregman method.

pixel being forced to one endmember. Note that the TV norm arranges the pixels so that similar materials are adjacent, forcing the purple anomaly to the bottom right corner of the image.

We then interpolated the 163-band Urban image by a factor of 4 using both the Endmember-Based and Quantum TV models. For the Urban image, we chose the parameters $\alpha = 1$ and $\beta = 10^{-4}$. Portions of the image are shown in Figures 4 and 5. Compared to the original image, the Endmember-Based TV image has less blocky and has more distinct edges. Fine-scale features such as the sidewalks and cars on the street are easier to see in the enhanced image. The colors in the Quantum TV image have changed significantly, because each pixel can only take on one of six colors specified by the endmember set. The image is a classification map with resolution 4 times larger than the original image. Note that features which were not represented by the endmember set, such as cars on the street, are not visible in the Quantum TV image. A more complete endmember basis would make these features visible and could potentially give rise to a subpixel anomaly detection algorithm.

Figure 3. Enhancement of a 177-band $2x2$ synthetic image with $4x$ zoom.

Figure 4. Enhancement of portion of the 163-band Urban image with 4x zoom - displayed as false color RGB image.

Figure 5. Enhancement of portion of the 163-band Urban image with 4x zoom - displayed as false color RGB image.

5. CONCLUSIONS

We proposed the LSL1 spectral unmixing model for finding a sparse representation of a hyperspectral signal in terms of its endmembers. This model can be solved very efficiently using Split Bregman iteration. We also showed how to use the spectral unmixing information to enhance the resolution of the hyperspectral image. We proposed two models based on the TV energy that incorporate the materials detected in the scene. The Endmember-Based TV model zooms and deblurs the image, while encouraging each pixel towards a pure state. The Quantum TV model produces a high resolution classification map that may provide more detail than a standard classification algorithm.

Future research on the LSL1 unmixing model could involve investigation of other numerical optimization schemes. In this paper, we assumed the endmember set was given. The LSL1 model may give some insight into the endmember selection problem, perhaps giving rise to an iterative selection and unmixing scheme similar to the paper by Rogge et al.[8] Also, extensive performance analysis and benchmarking against standard algorithms should be performed on real datasets.

For the resolution enhancement models, we assumed the blur function was a Gaussian and in our experiments we estimated the standard deviation. It may be possible to approach the deblurring as a blind deconvolution process or to obtain more precise information about the blur kernel from knowledge of the imaging system and atmospheric conditions. It would be interesting to compare the classification resulting from the Quantum TV model to the results of standard classification algorithms. It may also be possible to incorporate the resolution enhancement models into target and anomaly detection algorithms.

ACKNOWLEDGMENTS

The authors would like to thank Prof. Andrea Bertozzi, Tom Goldstein, and Michael Moeller for their advice. This research was supported by the Department of Defense.

REFERENCES

[1] M. Winter, E. Winter, S. Beaven, and A. Ratkowski, "Hyperspectral image sharpening using multispectral data," *IEEE Aerospace Conference 2007*, pp. 1-9, March 2007.

[2] M. Eismann and R. Hardie, "Hyperspectral resolution enhancement using high-resolution multispectral imagery with arbitrary response functions," *IEEE Trans. on Geoscience and Remote Sensing* **43:3**, March 2005.

[3] M. Winter and E. Winter, "Physics-based resolution enhancement of hyperspectral data," *Proc. SPIE Algorithms and Technologies for Multispectral, Hyperspectral, and Ultraspectral Imagery VIII* **4725**, pp. 580-587, 2002.

[4] M. Moeller, T. Wittman, and A.L. Bertozzi, "A variational approach to hyperspectral image fusion," *SPIE Conference on Defense, Security, and Sensing 2009*, April 2009.

[5] M. Winter, "N-FINDR: an algorithm for fast autonomous spectral end-member determination in hyperspectral data," *SPIE Conference on Imaging Spectrometry V* **3753**, 1999.

[6] J. Boardman, F. Kruse, and R. Green, "Mapping target signatures via partial unmixing of AVIRIS data," *Fifth Annual JPL Airborne Geoscience Workshop* **1**, 1995.

[7] C.-I. Chang, C.-C. Wu, W. Liu, and Y.-C. Ouyang. "A new growing method for simplex-based endmember extraction algorithm," *IEEE Trans. on Geoscience and Remote Sensing* **44**, pp. 2804-2819, 2006.

[8] D. Rogge, B. Rivard, J. Zhang, and J. Fang, "Iterative spectral unmixing for optimizing per-pixel endmember sets," *IEEE Trans. on Geoscience and Remote Sensing* **44:12**, pp. 3725-3736, 2006.

[9] A. Bateson and B. Curtiss, "A method for manual endmember selection and spectral unmixing," *Remote Sensing of Environment* **55**, pp. 229-243, 1996.

[10] B. Hapke, "Bidirection reflectance spectrocopy I: Theory," *J. Geophys. Res.* **86**, pp. 3039-3054, 1981.

[11] N. Keshave and J.F. Mustard, "Spectral unmixing," *Signal Processing Magazine* **19**, pp. 44-57, 2002.

[12] D.C. Heinz and C.-I Chang, "Fully constrained least squares linear spectral mixture analysis method for material quantification in hyperspectral imagery," *IEEE Trans. on Geoscience and Remote Sensing* **39:3**, pp. 529-545, March 2001.

[13] J.C. Harsanyi and C.-I Chang, "Hyperspectral image classification and dimensionality reduction: An orthogonal subspace projection approach," *IEEE Trans. on Geoscience and Remote Sensing*, **32:4**, pp. 779-785, July 1994.

[14] S. Osher, M. Burger, D. Goldfarb, J. Xu, and W. Yin, "An iterative regularization method for total variation based image restoration," *Multiscale Model. Simul.* **4(2)**, pp. 460-489, 2005.

[15] W. Yin, S. Osher, D. Goldfarb, and J. Darbon, "Bregman iterative algorithms for l1-minimization with applications to compressed sensing," *SIAM J. Imaging Sciences*,**1(1)**, pp. 143-168, 2008.

[16] T. Goldstein and S. Osher, "The split Bregman algorithm for L1 regularized problems," *UCLA CAM Report* **08-29**, 2008.

[17] L. Rudin, S. Osher, and E. Fatemi, "Nonlinear Total Variation based noise removal algorithms," *Physica D* **60**, pp. 259-268, November 1992.

[18] P.C. Hansen, "The L-curve and its use in the numerical treatment of inverse problems," *Computational Inverse Problems in Electrocardiology*, pp. 119-142, 2000.

[19] F. Malgouyres and F. Guichard, "Edge direction preserving image zooming: A mathematical and numerical analysis," *SIAM J. of Numerical Analysis* **39:1**, p. 1-37, 2001.

[20] D. Dobson and F. Santosa, "Recovery of blocky images from noisy and blurred data," *SIAM J. on Applied Mathematics* **56:4**, pp 1181-1198, August 1996.

[21] T.F. Chan and J. Shen, *Image Processing and Analysis*, SIAM, 2005.

[22] J. Shen and S.H. Kang, "Quantum TV and applications in image processing," *Inverse Problems and Imaging* **1:3**, pp. 557-575, 2007.

[23] US Army Corps of Engineers, Online: `http://www.tec.army.mil/Hypercurbe`.